A mechanoelectrical coupling model of neurons under stretching

Jin Tian[a,b,c,d,1], Guoyou Huang[b,c,1], Min Lin[b,c], Jinbin Qiu[b,c], Baoyong Sha[b,e], Tian Jian Lu[d,f,*], Feng Xu[b,c,**]

[a] State Key Laboratory for Strength and Vibration of Mechanical Structures, Xi'an Jiaotong University, Xi'an 710049, PR China
[b] The Key Laboratory of Biomedical Information Engineering of Ministry of Education, School of Life Science and Technology, Xi'an Jiaotong University, Xi'an 710049, PR China
[c] Bioinspired Engineering and Biomechanics Center (BEBC), Xi'an Jiaotong University, Xi'an 710049, PR China
[d] State Key Laboratory of Mechanics and Control of Mechanical Structures, Nanjing University of Aeronautics and Astronautics, Nanjing 210016, PR China
[e] Institute of Basic Medical Science, School of Basic Medical Science, Xi'an Medical University, Xi'an 710021, PR China
[f] Nanjing Center for Multifunctional Lightweight Materials and Structures (MLMS), Nanjing University of Aeronautics and Astronautics, Nanjing 210016, PR China

A R T I C L E   I N F O

A B S T R A C T

Neurons are situated in a microenvironment composed of various mechanical cues, where stretching is thought to have a major impact on neurons, resulting in microstructural changes in neural tissue and further leading to abnormal electrophysiological function. In spite of significant experimental efforts, the underlying mechanism remains elusive, more works are needed to provide a detailed description of the process that leads to the observed phenomena. Here, we developed a mechanoelectrical coupling model of central neurons under stretching and specially considered the plastic deformation of neurons. With the model, we showed that the increasing axial strain induces a decreased membrane action potential and a more frequent neuronal firing, which agree well with experimental observations reported in the literature. The simulation results also showed a faster electrophysiological signal conduction. Our model provides a reference for the prediction and regulation of neuronal function under simplified conditions of mechanical loadings.

1. Introduction

The central nervous system (CNS) performs many important functions *via* its electrophysiological behaviors, where central neurons are situated in a microenvironment composed of various biochemical and biophysical cues (Conway and Schaffer, 2014; Franze and Guck, 2010; Franze et al., 2013). In addition to biochemical cues that have been well studied, accumulating evidence has recently shown that mechanical cues (*e.g.*, stiffness, stretching) also have significant effects on central neuronal physiology (Feng et al., 2017; Franze and Guck, 2010; Franze et al., 2013). Stretching, one of the mechanical cues usually experienced by neurons, has been found to significantly affect neuron behaviors (Hill et al., 2016; Loverde and Pfister, 2015; Smith et al., 1999). During a moderate traumatic brain impact, the injury region in axons exhibits significant longitudinal strain (Shi and Pryor, 2002); and in a rat model of spinal cord injury, the most severe axonal injury is located

in the largest strain region (Fiford et al., 2004). Stretching may induce the alteration of axonal microstructure and macroscopic shape (Ahmadzadeh et al., 2014; Smith and Meaney 2000; Tang-Schomer et al., 2010), and even ion channel injury (Boucher et al., 2012; Volman and Ng, 2013; Wang et al., 2009a, 2009b). Moreover, the electrophysiological function of neurons is partly unrecoverable, even after removal of the loadings, possibly due to the irreversible damage to neuron cytoskeleton. Axons have long been considered as viscoelastic materials (Fung, 2013; Pioletti and Rakotomanana, 2000), while its plasticity has recently attracted attention (Bonakdar et al., 2016). Plastic deformation refers to the part of the deformation that cannot be recovered by itself after removal of the loading, which is considered to be caused by injury of the microstructure. For axons, plastic deformation is probably due to microtubule and tau protein disrupture. Therefore, the irreversible electrophysiological function lesion of axons may be related to its plastic deformation. Hence, it is of great

---

* Corresponding author at: State Key Laboratory of Mechanics and Control of Mechanical Structures, Nanjing University of Aeronautics and Astronautics, Nanjing 210016, PR China.
** Corresponding author at: The Key Laboratory of Biomedical Information Engineering of Ministry of Education, School of Life Science and Technology, Xi'an Jiaotong University, Xi'an 710049, PR China.
E-mail addresses: tjlu@nuaa.edu.cn (T.J. Lu), fengxu@mail.xjtu.edu.cn (F. Xu).
[1] Authors contributed equally to this work.
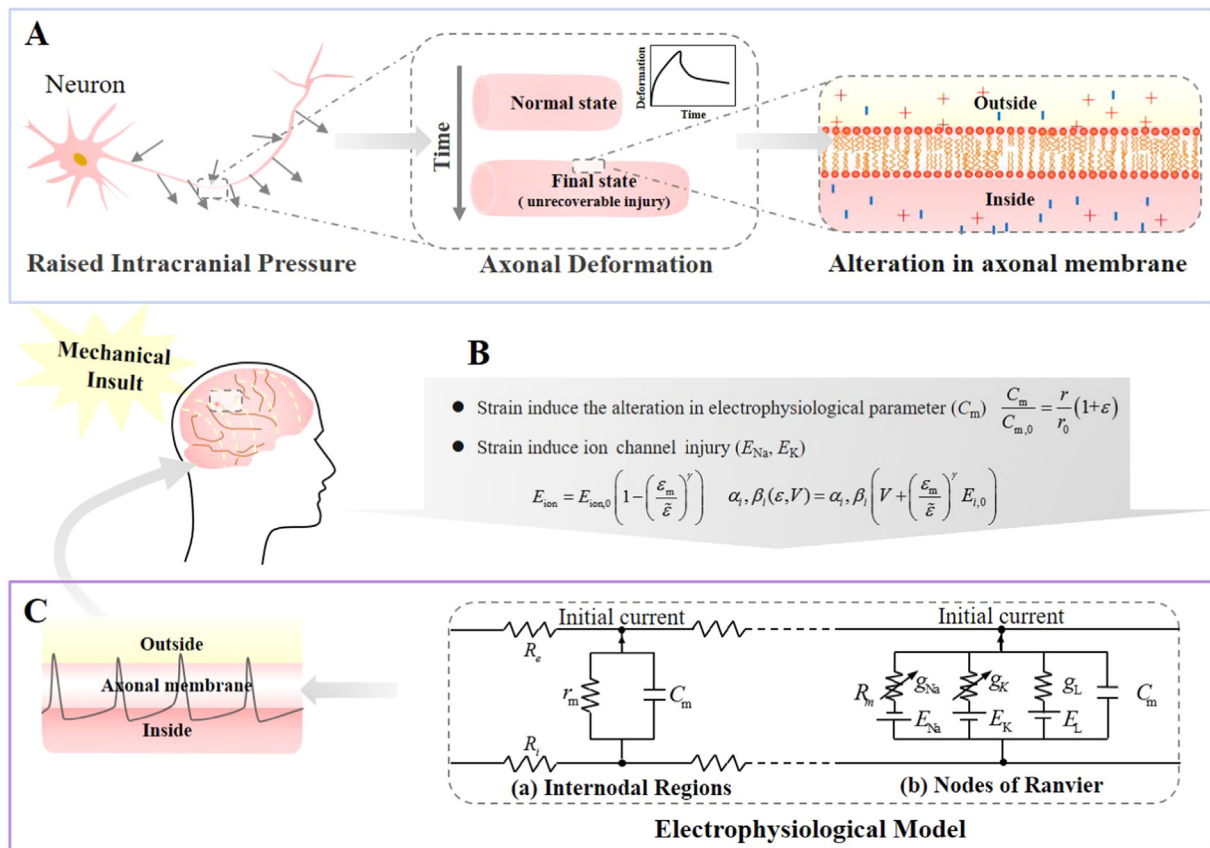
Fig. 1. Schematics of the mechanoelectrical coupling model of central neurons under stretching. The model consists of three submodels, *i.e.*, (A) the mechanical submodel, (B) the mechanoelectrical coupling submodel and (C) the electrophysiological submodel. The mechanical submodel deals with the relationship between mechanical loading and deformation of axons. The electrophysiological submodel characterizes the feature of AP based on two classical models (*i.e.*, the H-H model (b) and the cable theory (a)). The mechanoelectrical coupling submodel links the mechanical and electrophysiological submodels together through two aspects, *i.e.*, mechanical loading will alter the electrophysiological parameter (*i.e.*, the membrane capacitance) of the axonal equivalent circuit by changing axonal size (*i.e.*, the cell membrane area) (Jerusalem et al., 2014), and it will induce ion channel injury that can alter the ion channel equilibrium potential and rate constants (Jerusalem et al., 2014).

importance to understand the coupled mechanoelectrical behaviors of central neurons under stretching.

Significant efforts have been put toward experimentally studying the relationship between electrophysiological behaviors of neurons and stretching *in vitro* at both tissue level (Kang et al., 2015; Kang and Morrison, 2015a, 2015b) and cell level (Shi and Whitebone, 2006). For instance, at tissue level, Kang et al. applied biaxial stretch with strain level and strain rate relevant to traumatic brain injury on organotypic brain slices from various brain regions and investigated changes in electrophysiological activity of the brain slices (Kang et al., 2015; Kang and Morrison, 2015a, 2015b). They found that the alterations in electrophysiology were mostly dependent on strain and strain rate in a complicated way, while they were independent of brain anatomy. At the cell level, Shi et al. studied the conduction deficits of spinal cord axons under three different stretch strain levels (*i.e.*, $\varepsilon = 0.25$, $\varepsilon = 0.50$ and $\varepsilon = 1$) and two strain rate modes: slow stretching (strain rate from $0.006\,\mathrm{s}^{-1}$ to $0.008\,\mathrm{s}^{-1}$) and fast stretching (strain rate from $355\,\mathrm{s}^{-1}$ to $519\,\mathrm{s}^{-1}$) (Shi and Whitebone, 2006). They found that a higher strain level within each strain rate group, and a higher strain rate within each strain magnitude, both inflicted more damage. In addition to the experimental work of stretching axons, there are some studies focusing on the mechanisms of axonal injury. For example, Tang-Schomer et al. (2012) applied a dynamic stretching on cortical axons to determine the relationship between the integrity of regional microtubule and the formation of axonal varicosities. They found that primary microtubule failure may be a feature of diffuse axonal injury (DAI). Nevertheless, the underlying mechanism of the coupled mechanoelectrical behaviors of

central neurons remains elusive.

Mathematical modeling is a powerful tool that offers a quantitative description of the underlying mechanism of an observed biological phenomenon (Huang and Alben, 2016), including mechanical and electrophysiological behaviors of neurons. Ever since the ground-breaking work of Hodgkin and Huxley (1952), various mathematical models for neuroscience have been developed, which have helped us understand various neural behaviors, such as skin thermal pain (Xu and Lu, 2011). However, these models are often established from the perspectives of mechanics or electrophysiology separately, without appreciating the relationship between mechanical insult and electrophysiological function alteration of neurons. To address this shortcoming, several models have recently been developed to couple electrophysiological function alteration and mechanical insult together. For instance, Jérusalem et al. (2014) have developed an electromechanical coupling model associating electrophysiological impairment to structural damage as a function of strain level and strain rate. They directly linked mechanical loading and functional deficits through a damage criterion-based axonal deformation and deformation-induced parameter changes such as electric capacitance, conductance and equilibrium potential. Using this model, they have successfully simulated the propagation behavior of electrical signals under mechanical loading (Garcia-Grajales et al., 2015). However, they employed the damage criterion originated from metal materials in their model (Jerusalem et al., 2014), which may be different from biological tissues. Biological tissues are generally considered to be viscoelastic materials (Fung, 2013; Pioletti and Rakotomanana, 2000). Recent studies have

shown that after being subjected to mechanical loadings, the cells display not only a viscoelastic response but also plastic deformation (Bonakdar et al., 2016), which need to be considered in mathematical model to capture the native behavior of the axons under stretching. Tahereh et al. have developed a model by considering the relationship between neurons deformation (*i.e.*, the change in axonal shape) and neuronal electrophysiological alteration (Tekieh et al., 2016). However, this model treats neurons as inanimate objects, without considering the mechanically induced ion channel functional alterations.

As mentioned above, although injury to neurons is not only induced by stretching, stretching plays an important role in the injury of neurons. Thus, we simplified the loading conditions and developed a mechanoelectrical coupling model of neurons under stretching in this study. The model consists of three submodels, *i.e.*, the mechanical submodel (Fig. 1A), the mechanoelectrical coupling submodel (Fig. 1B) and the electrophysiological submodel (Fig. 1C). The mechanical submodel deals with the relationship between stretching and the deformation of axons, which has specially considered the plastic deformation of axons. The electrophysiological submodel characterizes the feature of neuronal action potential (AP), which is based on the classical H-H model and the cable theory. The mechanoelectrical coupling submodel links the mechanical and electrophysiological submodels through strain-induced equivalent circuit parameter alteration and ion channel injury. Considering that a large strain rate to axon may cause a wide range of MT breaks in the cytoskeleton (Wu and Adnan, 2018), in which the neurons almost completely lose its electrophysiological function, we only considered a small strain rate in our study to avoid the destruction of the cytoskeleton integrity. Besides, we have discussed a more general deformation condition, where an expanded model coupling the axonal deformation and electrophysiology alteration was explored. As the most essential parameters in an electrophysiological assessment, the amplitude of the AP, the neuronal firing frequency and the electrophysiological signal conduction velocity, which could be affected by mechanical cues, were used as outputs of the model. Our model provides a reference for the prediction and regulation of neuronal function under simplified conditions of mechanical loadings.

2. Development of the mathematical model

2.1. Mechanical submodel

Mechanical loadings can be generally decomposed into four basic forms, *i.e.*, stretching, compression, bending and twisting. The most destructive loading on neurons is stretching, since the compressive capacity of biological tissues is greater than the tensile capacity and the stress in the area of neuronal damage due to bending and twisting is mainly tensile stress. Therefore, we mainly studied the injury of central neurons under stretching.

The axons, as slender process on neurons that is responsible for conducting AP from the cell body, is one of the most important and vulnerable parts of neurons. Considering the fluid-like viscoelastic behavior of axons, the mechanical model of axons is usually represented by a structure consisting of a combination of springs and dampers that work together in parallel or in series, such as the Voigt model and the Maxwell model (Fung, 2013; Pioletti and Rakotomanana, 2000). We note that these viscoelastic models do not explain the issue of cell injury well. Recently, it was demonstrated that most living cells under mechanical loading show a viscoelastic deformation following a power law in time. After removing the mechanical loading, the cell deformation cannot be fully restored due to an additive plastic deformation, which follows the same power law as the completely reversible viscoelastic deformation (Bonakdar et al., 2016). By introducing the plastic deformation, Bonakdar *et al.* have considered cellular injury. They proposed that the total deformation of cells can be separated into two parts, *i.e.*, a viscoelastic part, $d_{ve}(t)$, and a plastic part, $d_{pl}(t)$

$$d(t) = d_{ve}(t) + d_{pl}(t) \tag{1}$$

Considering a power-law response with exponent β, the deformation during force application is

$$d(t) = (c_{ve} + c_{pl})\Delta F \left(\frac{t}{t_0}\right)^{\beta} \tag{2}$$

where c_{ve} and c_{pl} are the viscoelastic and plastic cell compliance, respectively, after a force duration of t_0.

The deformation after the removal of the force at $t = t_1$ is

$$d(t) = c_{ve}\Delta F \left[\left(\frac{t}{t_0}\right)^{\beta} - \left(\frac{t - t_1}{t_0}\right)^{\beta} \right] + c_{pl}\Delta F \left(\frac{t_1}{t_0}\right)^{\beta} \tag{3}$$

On the right side of Eq. (3), the first part describes the viscoelastic deformation, and the second part describes the plastic deformation. Where ΔF is the force step increase applied on cells; t is the time; t_0 is a reference time, which is set as 1 s; t_1 is the moment of force unloading; and β is the power-law exponent, with β = 0 indicating a purely elastic solid and β = 1 indicating a purely viscous fluid. β usually ranges from 0.1 to 0.5 in cells. Considering that the neurons we modeled are more compliant than usual cells, we set β as 0.65 according to the work of Grevesse et al. (2015).

In our simulation work, we are interested in the cell response after unloading. We notice that the coefficient $c_{ve}\Delta F$ of the viscoelastic term and the coefficient $c_{pl}\Delta F$ of the plastic term in Eq. (3) are constants when the loading form is determined. Therefore, the strain, defined by deformation divided by origin size, also follows the same power law as Eq. (3) in time. We take the power-law form of Eq. (3) and get the form of Eq. (4),

$$\varepsilon(t) = C_1 \left[\left(\frac{t}{t_0}\right)^{\beta} - \left(\frac{t - t_1}{t_0}\right)^{\beta} \right] + C_2 \left(\frac{t_1}{t_0}\right)^{\beta} \tag{4}$$

where C_1 and C_2 are the coefficients before the viscoelastic and plastic terms, respectively in Eq. (4).

2.2. Electrophysiological submodel

The electrophysiological submodel is composed of two classical models, *i.e.*, the Hodgkin-Huxley model (H-H model) and the cable theory (Fig. 1B). Due to the different characteristics of the nodes of Ranvier (NRs) and the myelinated internodal regions (IRs) (Koch and HC/Biologie, 1999), voltage-gated ion channels are mainly distributed at NRs, so the H-H model is applied at NRs to precisely describe the active generation and propagation of APs (Hodgkin and Huxley, 1952). In IRs, due to the multiple isolating myelin sheaths covering the axonal membrane, cable theory is employed here to describe the passive conduction of APs along the axons (Brzychczy and Poznanski, 2013; Koch and HC/Biologie, 1999).

The H-H model is given as (Hodgkin and Huxley, 1952):

$$C_m \frac{dV}{dt} = I - I_{ion} \tag{5}$$

where C_m is the capacitance of the axonal membrane per unit area in the radial direction; V is the displacement of the membrane AP from the resting voltage; t denotes time; I is a known external current applied on membrane, and I_{ion} is the current through ion channels. The ionic current is composed of sodium current (I_{Na}), potassium current (I_K) and a small "leakage current" (I_L) carried by chloride and other ions:

$$I_{ion} = g_{Na}(V - E_{Na}) + g_K(V - E_K) + g_L(V - E_L) \tag{6}$$

where g_{Na}, g_K and g_L are the conductance of ion channels, which can be expressed as Eq. (7). E_{Na} and E_K are the equilibrium potentials of the sodium and potassium ion channels, respectively. E_L is the equilibrium potential at which the "leakage current" due to chloride and other ions. L in g_L and E_L stands for leakage, which can refer to the H-H model

(Hodgkin and Huxley, 1952).

$$\begin{cases} g_{\text{Na}}(V) = \bar{g}_{\text{Na}} m^3 h \\ g_{\text{K}}(V) = \bar{g}_{\text{K}} n^4 \end{cases} \tag{7}$$

where $\bar{g}_{\text{Na}}$ and $\bar{g}_{\text{K}}$ are constants, which represent the maximum conductance of the Na^+ and K^+, respectively and have the dimensions of conductance per cm^2; and m, h and n are dimensionless variables which represent the opening possibility of ion channel, varying between 0 and 1. These parameters could be calculated through Eqs. (8)–(9):

$$\begin{cases} \frac{dm}{dt} = \alpha_{\text{m}}(1-m) - \beta_{\text{m}} m \\ \frac{dn}{dt} = \alpha_{\text{n}}(1-n) - \beta_{\text{n}} n \\ \frac{dh}{dt} = \alpha_{\text{h}}(1-h) - \beta_{\text{h}} h \end{cases} \tag{8}$$

$$\begin{cases} \alpha_{\text{m}} = \frac{0.1(V+40)}{1-e^{-0.1(V+40)}}, \quad \beta_{\text{m}} = 4e^{-0.0556(V+65)} \\ \alpha_{\text{n}} = \frac{0.01(V+55)}{1-e^{-0.1(V+55)}}, \quad \beta_{\text{n}} = 0.125e^{-0.0125(V+65)} \\ \alpha_{\text{h}} = 0.07e^{-0.05(V+65)}, \quad \beta_{\text{h}} = \frac{1}{1+e^{-0.1(V+35)}} \end{cases} \tag{9}$$

where α_{m}, α_{n} and α_{h} determine the rate of transfer from outside to inside, while β_{m}, β_{n} and β_{h} determine the rate of transfer from inside to outside. These rate constants are functions of voltage and do not vary with time, and they have the dimensions of [time] $^{-1}$ (Hodgkin and Huxley, 1952).

The cable theory is given as a second-order partial differential equation (Brzychczy and Poznanski, 2013; Koch and HC/Biologie, 1999):

$$C_{\text{m}} \frac{\partial V}{\partial t} = \frac{1}{R_{\text{e}} + R_{\text{i}}} \frac{\partial^2 V}{\partial z^2} + \frac{V}{r_{\text{m}}} \tag{10}$$

where R_{e} and R_{i} are extracellular and intracellular axial resistivity, respectively, z is the coordinate variable along the longitudinal direction of the axons, and r_{m} is the membrane resistivity per unit area, *i.e.*, $\frac{V}{r_{\text{m}}} = I_{\text{ion}}$. The parameters used in the electrophysiological submodel are listed in Table 1.

2.3. Coupling of the mechanical and electrophysiological submodel

The mechanoelectrical coupling model simulates the change in neuronal electrophysiological function of axons under mechanical loading. This coupling model couples mechanical cues and electrophysiological function mainly through two aspects. On the one hand, the mechanical loading alters electrophysiological parameter (*i.e.*, electrical capacitance) of the axonal equivalent circuit by changing axonal size (*i.e.*, cell membrane area) (Jerusalem et al., 2014). On the other hand, the mechanical loading induces ion channel injury that alters ion channel equilibrium potential and transfer rate constants (Jerusalem et al., 2014). Based on these two aspects, the electrophysiological parameters are not fixed but depend on stretching-induced deformation. Considering these two aspects, the AP on neuronal

Table 1
Parameters used in electrophysiological sub-model (Drapaca, 2015; Hodgkin and Huxley, 1952).

Symbol	Model parameters	Value
E_{Na}	Sodium potential	52.4 mV
E_{K}	Potassium potential	− 72.1 mV
E_{L}	Leakage potential	− 49.2 mV
$\bar{g}_{\text{Na}}$	Sodium conductance	120.0 m mho/cm^2
$\bar{g}_{\text{K}}$	Potassium conductance	36 m mho/cm^2
g_{L}	Leakage conductance	0.3 m mho/cm^2
C_{m}	Membrane capacitance	1.0 μF/cm^2
R_{i}	Resistivity of intracellular space	35 Ω cm
R_{e}	Resistivity of extracellular space	20 Ω cm

membrane is depicted following Eqs. (11)–(13).

When stretching is applied, the axial and radial sizes of the axons will change. We assume that the thickness of the axonal membrane (lipid bilayer) remains constant due to its fluidity. For the capacitance of the axonal membrane, consider a segment Δx along the axial direction of the axons, the area of the axonal membrane is $\pi d \Delta x$, where d denotes the diameter, and the thickness of the cell membrane is h_0 (h_0 is a constant). Simplifying the cell membrane into a parallel plate capacitor, the membrane capacitance is then in proportion to the surface area. Then, the relationship between the stretched capacitance and the initial capacitance is depicted following Eq. (11):

$$\frac{C_{\text{m}}}{C_{\text{m},0}} = \frac{2\pi r \Delta x}{2\pi r_0 \Delta x_0} = \frac{r}{r_0}(1+\varepsilon) \tag{11}$$

where r is the radius of the axons, the initial radius r_0 of the axons is set as 2 μm (Dayan and Abbott, 2005), and C_{m} is the capacitance of the axonal membrane per unit area in the radial direction. The initial value of C_{m} (*i.e.*, $C_{\text{m},0}$) is set as 1.0 μF/cm^2 (Hodgkin and Huxley, 1952).

Meanwhile, excessive strain can cause irreversible injury to ion channels, which has been demonstrated by the work of Wang et al. (2009a, 2009b), Boucher et al. (2012) and Volman and Ng (2013, 2015). These studies showed that mechanical strain can alter the probability of ion channels activation and inactivation, which is termed left shift (Fig. 3A). This implies altered ion channel conductivity and equilibrium potentials. Therefore, Jérusalem et al. have proposed that when mechanical strain is applied on the axons, the ion channel equilibrium potentials E_{Na} and E_{K} will decrease towards zero because of the increased leaking current as induced by the loss of membrane integrity.

The altered equilibrium potentials of each ion channel can be described by the following equations according to Jerusalem et al. (2014):

$$\begin{cases} E_{\text{Na}}(\varepsilon_{\text{m}}) = \begin{cases} E_{\text{Na},0}\left(1-\left(\frac{\varepsilon_{\text{m}}}{\tilde{\varepsilon}}\right)^\gamma\right), & if \quad \varepsilon_{\text{m}} < \tilde{\varepsilon} \\ 0, & else \end{cases} \\ E_{\text{K}}(\varepsilon_{\text{m}}) = \begin{cases} E_{\text{K},0}\left(1-\left(\frac{\varepsilon_{\text{m}}}{\tilde{\varepsilon}}\right)^\gamma\right), & if \quad \varepsilon_{\text{m}} < \tilde{\varepsilon} \\ 0, & else \end{cases} \end{cases} \tag{12}$$

where E_{Na} and E_{K} are the equilibrium potentials; the "0" in subscript of $E_{\text{Na},0}$ and $E_{K,0}$ denote the initial state of each parameter; γ is mechanical sensitive factor, and it was set as 2 according to Jerusalem et al. (2014); ε_{m} is axonal radial strain, which is equal to the ratio of the decrease in the axonal radius to the initial radius of the axons; and $\tilde{\varepsilon}$ denotes the injury criterial strain level of axons. Stretch-induced strain less than $\tilde{\varepsilon}$ is assumed to be recoverable, while the strain higher than $\tilde{\varepsilon}$ is partly unrecoverable due to the irreversible destruction of axonal microstructure. Here, $\tilde{\varepsilon}$ is set as 0.25 according to experimental data from Shi and Whitebone (2006).

To consider the left-shift effect in the H-H model, the rate constants α_i and β_i need to be modified. According to the work of Jerusalem et al. (2014), the parameters α_{m}, α_{h}, β_{m} and β_{h} are functions of $V - E_{\text{Na}}$, while α_{n} and β_{n} are functions of $V - E_{\text{K}}$, which denotes the difference between the membrane potential and the equilibrium potentials. The altered rate constants can be depicted by the following equations:

$$\begin{cases} \alpha_i(\varepsilon, V) = \begin{cases} \alpha_i\left(V + \left(\frac{\varepsilon_{\text{m}}}{\tilde{\varepsilon}}\right)^\gamma E_{i,0}\right), & if \quad \varepsilon_{\text{m}} < \tilde{\varepsilon} \\ \alpha_i(V + E_{i,0}), & else \end{cases} \\ \beta_i(\varepsilon, V) = \begin{cases} \beta_i\left(V + \left(\frac{\varepsilon_{\text{m}}}{\tilde{\varepsilon}}\right)^\gamma E_{i,0}\right), & if \quad \varepsilon_{\text{m}} < \tilde{\varepsilon} \\ \beta_i(V + E_{i,0}), & else \end{cases} \end{cases} \tag{13}$$

where i denotes Na and K; and $E_{i,0}$ is the corresponding equilibrium potential.

2.4. Simulation steps and boundary conditions

In our simulation, we first applied axial stretching on the axons. To be consistent with the process reported in the literature (Shi and Whitebone, 2006), we stretched the axons with a constant strain rate of 0.007 per second while the axons did not adhere to the substrate. The initial radius of the axons is set as $2\,\mu m$. Corresponding to three different maximum strain levels (0.25, 0.5 and 1.0), we calculated each axonal deformation, and further got the axonal radius. The coefficients C_1 and C_2 are set as 0.0066 and 0.0086, respectively. Next, we applied the radius of the axons after stretching to the coupling submodel to calculate the new membrane capacitance, the ion channel equilibrium potentials and the ion channel rate constants. With this, we got the modified electrical parameters in the H-H model and the cable theory.

The Hodgkin–Huxley equations, *i.e.*, Eqs. (5)–(9), were solved with the following initial conditions (Drapaca, 2015; Hodgkin and Huxley, 1952):

$$V(0) = -65\text{mV}, \qquad m(0) = \frac{\alpha_m(V(0))}{\alpha_m(V(0)) + \beta_m(V(0))},$$

$$n(0) = \frac{\alpha_n(V(0))}{\alpha_n(V(0)) + \beta_n(V(0))}, \qquad h(0) = \frac{\alpha_h(V(0))}{\alpha_h(V(0)) + \beta_h(V(0))} \qquad (14)$$

By solving the partial differential equation using MATLAB (R2016b), the distribution of AP with time and position was obtained.

3. Results

To understand the mechanoelectrical coupling of central neurons under stretching, we developed a mechanoelectrical coupling model, which consists of the mechanical submodel (Fig. 1A), the mechanoelectrical coupling submodel (Fig. 1B) and the electrophysiological submodel (Fig. 1C).

To verify our mechanoelectrical coupling model, we simulated the electrophysiological behaviors of an axon under stretching with a low strain rate (Fig. 2A), following the experimental study in the literature (Shi and Whitebone, 2006). The axon has a length of 10 mm, and the loading is applied at a relatively low strain rate of $0.007\,\text{s}^{-1}$. We simulated three maximum stretch-induced strain levels (*i.e.*, $\varepsilon = 0.25$, $\varepsilon = 0.5$ and $\varepsilon = 1$) to test the effect of maximum strain on neuronal electrophysiology (Fig. 2B). Then, we extracted the peak AP at the distal end of the axon and tracked for 30 min after the removal of stretching. We observed that the peak AP decreases gradually with increasing strain.

The AP represents the degree of neuronal excitement (an important function of the nervous system). A greater loss of AP indicates a greater loss of neuronal excitability and thus functionality. Thus, as the strain increases, the function of the nervous system declines faster. Moreover, the reduced AP can no longer be restored to the original peak, implying that the damage after stretching eventually becomes irreversible. We also extracted the peak AP of the axons from the experimental work of Shi and Whitebone (data extracted from Fig. 2B of their paper) (Shi and Whitebone, 2006). We compared the simulation results with the experimental data and observed a good agreement (Fig. 2C).

Our simulation results also show firing rates and conduction velocity of AP along axons under different loading states. In addition to a decreased membrane peak AP, strain also induces a more frequent neuronal firing (Fig. 3A) and a faster conduction (Fig. 3B). In Fig. 3A, the four colored curves represent the APs at the distal end of the axon, corresponding to the four strain levels as a function of time. Due to the alternation of the probability of ion channel activation and inactivation under mechanical loading, we can observe the left shift of the AP. This also means that the duration of neuronal firing is shorter, *i.e.*, a more frequent firing. These observations are consistent with the reported works (Boucher et al., 2012; Volman and Ng, 2013, 2015; Wang et al., 2009a, 2009b). In Fig. 3B, the bright lines represent the spot where the AP reaches its maximum magnitude. The conduction velocity of AP is reflected by the slope of the bright lines, where higher slope means
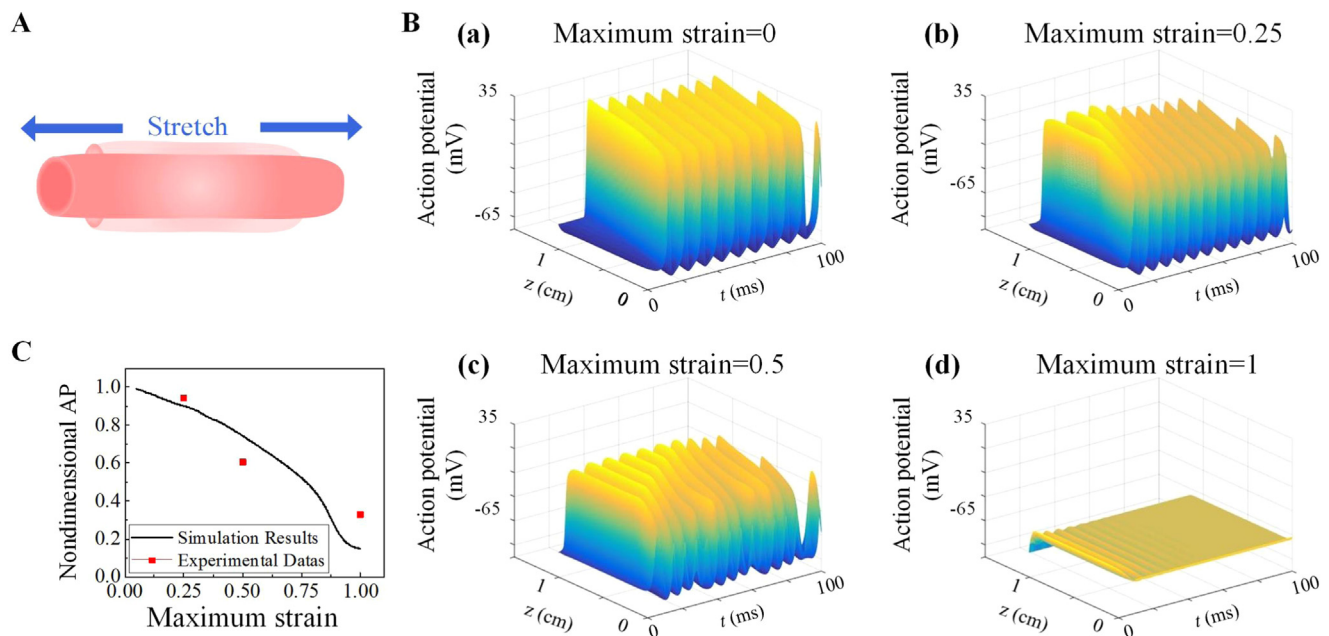
Fig. 2. Comparison of the mechanoelectrical coupling model with experimental data from the literature. Three loading states of various maximum strain (0.25, 0.5 and 1 at the strain rate of $0.007\,\text{s}^{-1}$) were simulated, and axonal responses in three situations were calculated and compared with reported experiments (Shi and Whitebone, 2006). Panel (A) denotes the form of stretch loading. After unloading, the amplitude of the AP of the axon was measured. Panel (B) is the simulated space-time distribution of AP. The *z*-axis represents the spatial coordinates along the axis of the axon, and the *t*-axis represents time. The vertical axis represents the AP at a particular moment and position. When the *z*-coordinate is fixed, the resulting curve represents the time-dependent change in the AP of a fixed point on the axon. When the *t*-axis is fixed, the AP distribution of each point on the whole axon is obtained at a certain fixed time. Panel (C) is the comparison of the simulation results with the experimental data reported in the literature (Shi and Whitebone, 2006). Here, the AP peak value of the healthy axons in the nonstretched state is taken as the standard, and the ratio of the AP amplitude in the other loading states to the standard value is used as a measure of the loss of the axon function.

A

B
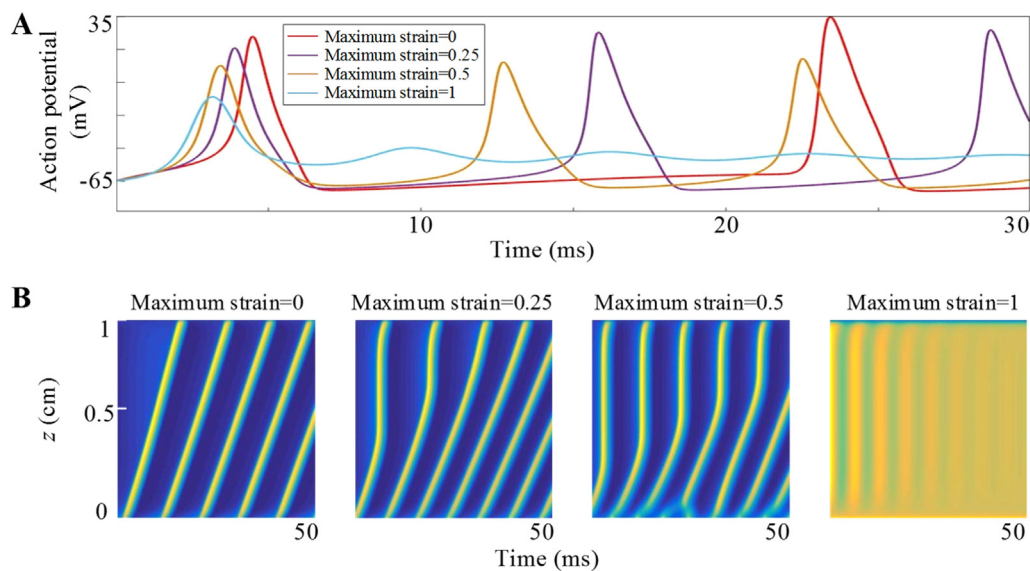
Fig. 3. The axonal AP firing rates and conduction velocity under stretching. (A-B) The simulated time-space distribution of the amplitude of AP. (A) APs at the distal end of the axon corresponding to the four strain levels as a function of time. (B) Conduction velocity of APs under four strain levels. The t-axis, z-axis and bright lines represent time, the position on the axon and the spot where AP reaches its maximum magnitude, respectively.

higher conduction velocity. The simulation showed that the conduction velocity and the stretch-induced strain exhibit a positive correlation.

It is worth noting that the simulation results of Jerusalem et al. (2014) and ours are both consistent with the experimental results in literature (Shi and Whitebone, 2006). However, the two works are different in some aspects. Firstly, in the mechanical submodel, Jerusalem et al. treated axons as viscoelastic material and introduced a damage evolution equation as inspired by metal plasticity yield evolution rules, while we considered the plastic deformation of the axons to further recapitulate complex mechanical properties of native axons and linked this irreversible deformation to the injury of the axons. Secondly, in the coupling submodel, strain-induced modification of the circuit parameters was considered, but we took a different form from that of Jerusalem et al. They considered this issue from a microscopic view, while we linked the strain and circuit parameters directly by axonal radius, as reflected in Eq. (11). Finally, a more general necking deformation case was investigated in our study, which coupled axonal deformation and electrophysiology, as will be discussed in Section 4.1. Therefore, we expect our model can help to capture the native mechanoelectrical behavior of axons and promote the development of neuroscience research.

4. Discussion

4.1. Complicated loading-induced electrophysiological alteration

In a realistic situation, the mechanical loading borne by neurons is very complicated. For example, neurons may suffered traumatic brain injury (TBI) due to short-term intensive loads; neurons may endure changes in the stiffness of the brain tissue due to disease, such as Alzheimer's disease, which causes a decrease in the stiffness of brain tissue (Franze et al., 2013); ultrasound can also functionally modulate neuronal activity (Deffieux et al., 2013; Fry et al., 1958; King et al., 2013; Tufail et al., 2010). These will change the microenvironment of neurons, causing a series of changes in their electrophysiology. In the above study, we have chosen stretching as the main loading since biological tissues are more sensitive to tension than to compression (Fung, 2013; Pioletti and Rakotomanana, 2000). Nevertheless, other forms of mechanical loading are also important, which may induce complex deformation of the axons (*e.g.*, necking and swelling along the axons). Moreover, N.S. Gov has carried out a comprehensive work demonstrating that the width distribution of the axons varies along the axial direction (Gov, 2009).

To consider a more realistic situation, we assumed that the axons

are deformed due to combined mechanical loadings composed of stretching, compression, bending and twisting. In this case, the cross-sectional radius of the axons varies along the axial direction. Due to the complexity and uncertainty of loading, it is hard to give a uniform force-deformation expression here. However, as long as the physical property parameters, loadings and boundary conditions of the axons are determined, the mechanical-induced axonal longitudinal deformation can be obtained using the finite element method. Thus, the axonal radius along the axis direction can be described by a function of z. According to our mechanoelectrical coupling submodel, the change in radius will cause changes in the parameters C_m, E_{Na}, E_K and E_L. In addition, such variation of the radius along the axons will change the propagation behavior of APs. Taking a small piece of microelement along the axis on the deformed axons, because $ds^2 = dr^2 + dz^2$, we have

$$\frac{ds}{dz} = \sqrt{1 + \left(\frac{dr}{dz}\right)^2} \tag{15}$$

Combining Eq. (10) with Eq. (15), we can deduce the conduction law of APs in a deformed axon:

$$\left(C_m \frac{\partial V}{\partial t} + I_{ion}\right)\frac{ds}{dz} = \frac{r}{2(R_e + R_i)}\frac{\partial^2 V}{\partial z^2} + \frac{1}{R_e + R_i}\frac{dr}{dz}\frac{\partial V}{\partial z} \tag{16}$$

To study the necking caused by these combined loadings, we took the simplest form of the curve, *i.e.*, a quadratic function. As shown in Fig. 4A, the deformation of an axon is a symmetrical distribution, with the vertical necking deformation of the middle cross section Δh reflecting the magnitude of the overall deformation of the axon. We can obtain the longitudinal section of different shapes by adjusting the parameter values of A, B and C:

$$r(z) = A - Bz - Cz^2 \tag{17}$$

To study the effects of such necking deformation on neuronal function, we simulated the electrophysiological behaviors of an axon under each necking state (Fig. 4B). We observed that the bright lines (the spot where AP reaches its maximum magnitude) in Fig. 4B are remarkably curved in the middle region, in contrast to those in Fig. 3, mainly due to the necking of the axons in its middle region. We also observed that the AP amplitude decreases at the necking region and recovers after that, indicating a blockage of the AP. This may be due to an irreversible change in microstructure, such as molecular bonds in the necking region (Ahmadzadeh et al., 2014). We further extracted the average conduction velocity of the AP in the middle region of the axons (0.45–0.55 mm length range) under different deformed states (Fig. 4C).
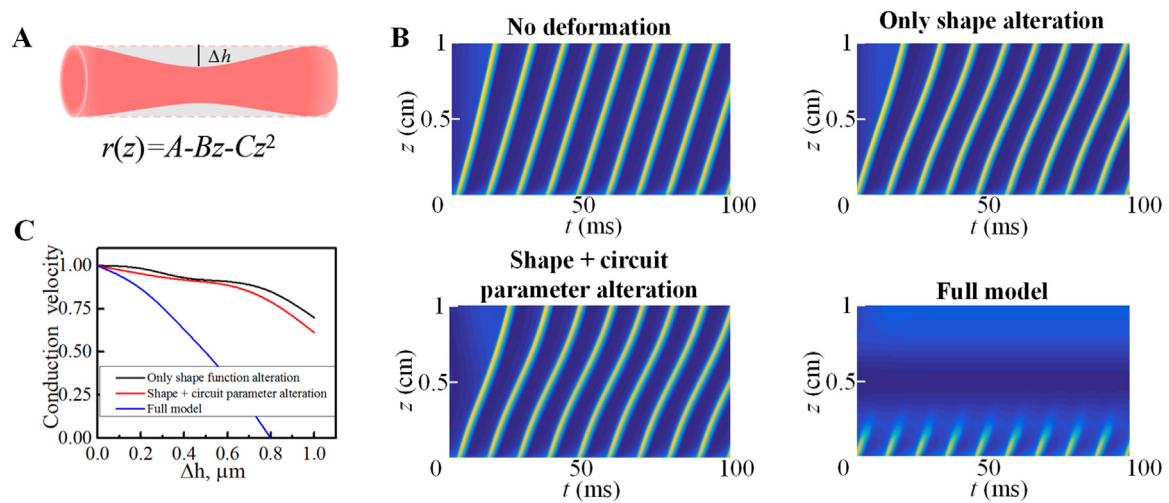
Fig. 4. Prediction of axonal conduction velocity under general mechanical loading. (A) The form of the general mechanical loading, where the axons narrows in the middle region due to combined mechanical loading. (B) Simulated time-space distribution of maximum AP under each maximum deformation. The t-axis, z-axis and bright lines represent the time axis, the position on the axons and the spot where AP reaches its maximum magnitude, respectively. (C) Prediction of the relationship between the conduction velocity and the maximum strain, where the black line represents the simulation result only considering axonal shape alteration, the red line represents the simulation result without considering ion channel injury, and the blue line represents the simulation result by considering ion channel injury.

We observed that the conduction velocity decreases with the increase in deformation degree, which is consistent with the results reported by Galbraith et al. (1993). We also studied the effects of the three factors (*i.e.*, shape alteration, equivalent circuit parameter alteration and ion channel injury) on our model. We observed that injury to the ion channel has most essential effect on the electrophysiology (Fig. 4C), which implies the significance of ion channels in neuronal electrophysiology, as has been reported experimentally (Wang et al., 2009a, 2009b).

4.2. Microenvironment of neurons

In addition to being subjected to external forces, neurons also actively perceive the surrounding mechanical microenvironment. For instance, substrate nanotopography can change the physiological behavior of neurons (Migliorini et al., 2011); neurons cultured on differently coated surfaces present individual adhesion patterns and morphologies (Sun et al., 2012). Neurons have a tendency to grow better on softer substrates (Georges et al., 2006; Sorkin et al., 2009; Sun et al., 2012). Moreover, the gradient of substrate stiffness can influence the direction of axonal bending (Franze et al., 2009; Koser et al., 2016). These processes are thought to be related to the perception by the growth cone of its mechanical microenvironment. Chan and Odde have proposed a molecular clutch model and used it to successfully explain the spreading of neuronal filopodia on compliant substrates (Chan and Odde, 2008).

The growth cone exerts a towed force on the axons, leading to axonal towed growth (Dennerll et al., 1989; Lamoureux et al., 1989). O'Toole and Miller et al. further suggest that this towed force will promote slow axonal transport over a longer time (O'Toole and Miller, 2011). The simulation works from Rooij et al. have also shown the dynamic changes to the cytoskeleton, such as the polymerization and depolymerization of microtubules and the attachment and detachment between tau protein and microtubules, which indicate the significance of protein transport along the axons (De and Kuhl, 2018; Rooij et al., 2017). Therefore, the mechanical microenvironment can also exert a pulling force on the axons through the perception of the growth cone and promote slow axonal transport, thereby altering the structure and function of the neuron.

4.3. Axonal volume increase

Mechanical cues contribute to the transport of biomass within an axon. For instance, Pfister et al. found that when stretching is applied to axons, the axons can be stretched at a rate of 8 mm/day for approximately 7 days without thinning (Pfister et al., 2006, 2004). This implies that under certain situations, stretching will help to promote slow axonal transport. Moreover, there is a large body of evidence showing that axons increase in diameter under the normal physiological state. For example, the diameter of the human sural nerve is approximately 0.28 μm in infants and will increase to approximately 0.44 μm in adults (Jacobs and Love, 1985). Increases in axonal diameter are also observed in Drosophila, chick and rat neurons (Hoffman et al., 1986; Lamoureux et al., 2010; O'Toole et al., 2008). As a result, the increase in axonal length and diameter, as well as degradation of proteins along the axons, requires slow axonal transport to meet the demand for new protein. Stretching promotes slow axonal transport (O'Toole and Miller, 2011; Purohit and Smith, 2016). However, a recent work pointed out that axons do not always increase volume under sustained strain (Fan et al., 2017). This suggests a different mechanism underlying the different loading conditions. We noticed that when the loading is applied slowly, the volume of the axons increases, and when the loading is applied quickly, the volume of the axons remains unchanged. This indicates that stretching with different strain rates will result in different microtubule (MT) dynamics, *i.e.*, when stretch is applied at a rate higher than the polymerization process, MTs will break and subsequently disassemble (Fan et al., 2017).

In our simulation work, the simulated strain rate ($\sim 0.007\,\mathrm{s}^{-1}$) is much slower than the fast strain rate of 355–$519\,\mathrm{s}^{-1}$ applied in the study of Shi and Whitebone (2006), so MTs in axons may not break and there might be biomass transport during stretching. However, since the loading lasts for a very short time (~ 35.7–$142.8\,\mathrm{s}$), we assume that the biomass transport due to the loading is negligible.

4.4. Limitations and future work

Firstly, as mentioned above, the time scales we consider in our work are still relatively short. In some studies, the stretching on the neurons can last for several days, such as the work of Pfister et al. (2006, 2004). When neurons are cultured on a two-dimensional substrate, the growth cone forms a bond with substrate and exerts a pulling force on the

neurons. This stretching elongates neurons for several days, which is called towed growth, corresponding to a longer time scale. At these longer time scales, the biomass transport process along the axons needs to be considered. Our future work will explore this issue. Secondly, we also notice that the performance of cells in the three-dimensional (3D) environment is different from that of two-dimensional, especially the neurons are actually in a 3D mechanical microenvironment *in vivo*. Our future efforts will employ finite element methods to establish a 3D mechanoelectrical coupling model for neurons. Thirdly, there are no experimental observations to support the proposed physically relevant expressions for key electrophysiological and mechanical parameters in our model, such as Eq. (4) and Eq. (11). Eq. (4) is derived according to the work of Bonakdar et al. (2016), in which the coefficients C_1 before viscoelastic and C_2 before plastic terms are estimated values that vary with strain and strain rate. The Eq. (11) is derived based on the assumption that the cell membrane can be simplified into a parallel plate capacitor. However, we expect that our simplified model will inspire future experimental work that can provide empirical relationships among neuronal electrophysiological and mechanical parameters.

5. Conclusion

In this study, we developed a mechanoelectrical coupling model of central neurons under stretching with consideration of axonal plastic deformation. With the model, we found that the effect of mechanical loading on electrophysiology mainly manifests as decreased membrane AP amplitude, a more frequent neuronal firing and a faster electrophysiological signal conduction. The model predicts not only stretch-induced injury but also a more general necking deformation case, which may someday be revealed in future by experiments, providing a reference for the prediction and regulation of neuronal function under mechanical loadings.

Acknowledgment

Author contributions

Feng Xu and Tian Jian Lu contributed to the conceptualization and funding acquisition. Jin Tian and Guoyou Huang performed formal analysis, methodology, writing original draft and writing- review & editing. Min Lin, Jinbin Qiu and Baoyong Sha contributed to the conceptualization of the study and commented on the manuscript.

Competing interests

The authors declare that they have no competing interests.

References

Ahmadzadeh, H., Smith, D.H., Shenoy, V.B., 2014. Viscoelasticity of tau proteins leads to strain rate-dependent breaking of microtubules during axonal stretch injury: predictions from a mathematical model. Biophys. J. 106 (5), 1123–1133.

Bonakdar, N., Gerum, R., Kuhn, M., Spörrer, M., Lippert, A., Schneider, W., Fabry, B., 2016. Mechanical plasticity of cells. Nat. Mater. 15 (10).

Boucher, P.A., Joós, B., Morris, C.E., 2012. Coupled left-shift of Nav channels: modeling the Na⁺-loading and dysfunctional excitability of damaged axons. J. Comput. Neurosci. 33 (2), 301–319.

Brzychczy, S., Poznanski, R.R., 2013. Mathematical Neuroscience. Academic Press.

Chan, C.E., Odde, D.J., 2008. Traction dynamics of filopodia on compliant substrates. Science 322 (5908), 1687–1691.

Conway, A., Schaffer, D.V., 2014. Biomaterial microenvironments to support the generation of new neurons in the adult brain. Stem Cells 32 (5), 1220–1229.

Dayan, P., Abbott, L., 2005. Theoretical neuroscience: computational and mathematical modeling of neural systems. Philos. Psychol. 15 (1), 154–155.

De, R.R., Kuhl, E., 2018. Microtubule Polymerization and cross-link dynamics explain Axonal stiffness and damage. Biophys. J. 114 (1), 201–212.

Deffieux, T., Younan, Y., Wattiez, N., Tanter, M., Pouget, P., Aubry, J.-F., 2013. Low-intensity focused ultrasound modulates monkey visuomotor behavior. Curr. Biol. 23 (23), 2430–2433.

Dennerll, T.J., Lamoureux, P., Buxbaum, R.E., Heidemann, S.R., 1989. The cytomechanics of axonal elongation and retraction. J. Cell Biol. 109 (6), 3073–3083.

Drapaca, C.S., 2015. An electromechanical model of neuronal dynamics using Hamilton's principle. Front. Cell. Neurosci. 9, 271.

Fan, A., Tofangchi, A., Kandel, M., Popescu, G., Saif, T., 2017. Coupled circumferential and axial tension driven by actin and myosin influences in vivo axon diameter. Sci. Rep. 7 (1), 14188.

Feng, X.-Q., Lee, P.V.S., Lim, C.T., 2017. Preface: molecular, cellular, and tissue mechanobiology. Acta Mech. Sin. 33 (2), 219–221.

Fiford, R., Bilston, L., Waite, P., Lu, J., 2004. A vertebral dislocation model of spinal cord injury in rats. J. Neurotrauma 21 (4), 451–458.

Franze, K., Gerdelmann, J., Weick, M., Betz, T., Pawlizak, S., Lakadamyali, M., Lu, Y.B., 2009. Neurite branch retraction is caused by a threshold-dependent mechanical impact. Biophys. J. 97 (7), 1883.

Franze, K., Guck, J., 2010. The biophysics of neuronal growth. Rep. Prog. Phys. 73 (9), 094601.

Franze, K., Janmey, P.A., Guck, J., 2013. Mechanics in neuronal development and repair. Annu. Rev. Biomed. Eng. 15, 227–251.

Fry, F., Ades, H., Fry, W., 1958. Production of reversible changes in the central nervous system by ultrasound. Science 127 (3289), 83–84.

Fung, Y.-C., 2013. Biomechanics: Mechanical Properties of Living Tissues. Springer Science & Business Media.

Galbraith, J., Thibault, L., Matteson, D., 1993. Mechanical and electrical responses of the squid giant axon to simple elongation. Trans.-Am. Soc. Mech. Eng. J. Biomech. Eng. 115 (13-13).

Garcia-Grajales, J.A., Rucabado, G., Garcia-Dopico, A., Pena, J.M., Jerusalem, A., 2015. Neurite, a finite difference large scale parallel program for the simulation of electrical signal propagation in neurites under mechanical loading. PLoS One 10 (2), e0116532.

Georges, P.C., Miller, W.J., Meaney, D.F., Sawyer, E.S., Janmey, P.A., 2006. Matrices with compliance comparable to that of brain tissue select neuronal over glial growth in mixed cortical cultures. Biophys. J. 90 (8), 3012–3018.

Gov, N.S., 2009. Physical model for the width distribution of axons. Eur. Phys. J. E Soft Matter 29 (3), 337.

Grevesse, T., Dabiri, B.E., Parker, K.K., Gabriele, S., 2015. Opposite rheological properties of neuronal microcompartments predict axonal vulnerability in brain injury. Sci. Rep. 5, 9475.

Hill, C.S., Coleman, M.P., Menon, D.K., 2016. Traumatic axonal injury: mechanisms and translational opportunities. Trends Neurosci. 39 (5), 311–324.

Hodgkin, A.L., Huxley, A.F., 1952. A quantitative description of membrane current and its application to conduction and excitation in nerve. J. Physiol. 117 (4), 500.

Hoffman, S., Friedlander, D.R., Chuong, C.M., Grumet, M., Edelman, G.M., 1986. Differential contributions of Ng-CAM and N-CAM to cell adhesion in different neural regions. J. Cell Biol. 103 (1), 145–158.

Huang, W.-X., Alben, S., 2016. Fluid–structure interactions with applications to biology. Acta Mech. Sin. 32 (6), 977–979.

Jacobs, J.M., Love, S., 1985. Qualitative and quantitative morphology OF human sural nerve at different ages. Brain J. Neurol. 108 (Pt 4), 897 (4).

Jerusalem, A., Garcia-Grajales, J.A., Merchan-Perez, A., Pena, J.M., 2014. A computational model coupling mechanics and electrophysiology in spinal cord injury. Biomech. Model Mechanobiol. 13 (4), 883–896.

Kang, W.H., Cao, W., Graudejus, O., Patel, T.P., Wagner, S., Meaney, D.F., Morrison 3rd, B., 2015. Alterations in hippocampal network activity after in vitro traumatic brain injury. J. Neurotrauma 32 (13), 1011–1019.

Kang, W.H., Morrison III, B., 2015a. Functional tolerance to mechanical deformation developed from organotypic hippocampal slice cultures. Biomech. Model. Mechanobiol. 14 (3), 561–575.

Kang, W.H., Morrison III, B., 2015b. Predicting changes in cortical electrophysiological function after in vitro traumatic brain injury. Biomech. Model. Mechanobiol. 14 (5), 1033–1044.

King, R.L., Brown, J.R., Newsome, W.T., Pauly, K.B., 2013. Effective parameters for ultrasound-induced in vivo neurostimulation. Ultrasound Med. Biol. 39 (2), 312–331.

Koch, C., HC/Biologie, 1999. Biophysics of Computation. Oxford University Press.

Koser, D.E., Thompson, A.J., Foster, S.K., Dwivedy, A., Pillai, E.K., Sheridan, G.K., Guck, J., 2016. Mechanosensing is critical for axon growth in the developing brain. Nat. Neurosci. 19 (12), 1592.

Lamoureux, P., Buxbaum, R.E., Heidemann, S.R., 1989. Direct evidence that growth cones pull. Nature 340 (6229), 159–162.

Lamoureux, P., Heidemann, S.R., Martzke, N.R., Miller, K.E., 2010. Growth and elongation within and along the axon. Dev. Neurobiol. 70 (3), 135–149.

Loverde, J.R., Pfister, B.J., 2015. Developmental axon stretch stimulates neuron growth while maintaining normal electrical activity, intracellular calcium flux, and somatic morphology. Front. Cell. Neurosci. 9, 308.

Migliorini, E., Grenci, G., Ban, J., Pozzato, A., Tormen, M., Lazzarino, M., Ruaro, M.E., 2011. Acceleration of neuronal precursors differentiation induced by substrate nanotopography. Biotechnol. Bioeng. 108 (11), 2736–2746.

O'Toole, M., Latham, R., Baqri, R.M., Miller, K.E., 2008. Modeling mitochondrial dynamics during in vivo axonal elongation. J. Theor. Biol. 255 (4), 369.

O'Toole, M., Miller, K.E., 2011. The role of stretching in slow axonal transport. Biophys. J. 100 (2), 351–360.

Pfister, B.J., Bonislawski, D.P., Smith, D.H., Cohen, A.S., 2006. Stretch-grown axons retain the ability to transmit active electrical signals. FEBS Lett. 580 (14), 3525–3531.

Pfister, B.J., Iwata, A., Meaney, D.F., Smith, D.H., 2004. Extreme stretch growth of integrated axons. J. Neurosci. 24 (36), 7978–7983.

Pioletti, D.P., Rakotomanana, L.R., 2000. Non-linear viscoelastic laws for soft biological tissues. Eur. J. Mech. A-Solids 749–759 (19(LBO-Artic.-2000-002)).

Purohit, P.K., Smith, D.H., 2016. A model for stretch growth of neurons. J. Biomech. 49 (16), 3934–3942.

Rooij, R., Miller, K.E., Kuhl, E., 2017. Modeling Molecular Mechanisms in the Axon. Springer-Verlag New York, Inc.

Shi, R., Pryor, J., 2002. Pathological changes of isolated spinal cord axons in response to mechanical stretch. Neuroscience 110 (4), 765–777.

Shi, R., Whitebone, J., 2006. Conduction deficits and membrane disruption of spinal cord axons as a function of magnitude and rate of strain. J. Neurophysiol. 95 (6), 3384–3390.

Smith, D.H., Wolf, J.A., Lusardi, T.A., Lee, V.M.-Y., Meaney, D.F., 1999. High tolerance and delayed elastic response of cultured axons to dynamic stretch injury. J. Neurosci. 19 (11), 4263–4269.

Sorkin, R., Greenbaum, A., David-Pur, M., Anava, S., Ayali, A., Ben-Jacob, E., Hanein, Y., 2009. Process entanglement as a neuronal anchorage mechanism to rough surfaces. Nanotechnology 20 (1), 015101.

Sun, Y., Huang, Z., Liu, W., Yang, K., Sun, K., Xing, S., Jiang, X., 2012. Surface coating as a key parameter in engineering neuronal network structures in vitro. Biointerphases 7 (1–4), 29.

Tang-Schomer, M.D., Johnson, V.E., Baas, P.W., Stewart, W., Smith, D.H., 2012. Partial interruption of axonal transport due to microtubule breakage accounts for the formation of periodic varicosities after traumatic axonal injury. Exp. Neurol. 233 (1), 364–372.

Tekieh, T., Shahzadi, S., Rafii-Tabar, H., Sasanpour, P., 2016. Are deformed neurons electrophysiologically altered? A simulation study. Curr. Appl. Phys. 16 (10), 1413–1417.

Tufail, Y., Matyushov, A., Baldwin, N., Tauchmann, M.L., Georges, J., Yoshihiro, A., Tyler, W.J., 2010. Transcranial pulsed ultrasound stimulates intact brain circuits. Neuron 66 (5), 681–694.

Volman, V., Ng, L.J., 2013. Computer modeling of mild axonal injury: implications for axonal signal transmission. Neural Comput. 25 (10), 2646–2681.

Volman, V., Ng, L.J., 2015. Perinodal glial swelling mitigates axonal degradation in a model of axonal injury. J. Neurophysiol. 115 (2) (jn.00912.02015).

Wang, J.A., Lin, W., Morris, T., Banderali, U., Juranka, P.F., Morris, C.E., 2009a. Membrane trauma and Na + leak from Nav1.6 channels. Am. J. Physiol. Cell Physiol. 297 (4), 823–834.

Wang, J.A., Lin, W., Morris, T., Banderali, U., Juranka, P.F., Morris, C.E., 2009b. Membrane trauma and Na + leak from Nav1. 6 channels. Am. J. Physiol.-Cell Physiol. 297 (4), C823–C834.

Wu, Y.-T., Adnan, A., 2018. Damage and failure of axonal microtubule under extreme high strain rate: an in-silico molecular dynamics study. Sci. Rep. 8 (1), 12260.

Xu, F., Lu, T., 2011. Introduction to Skin Biothermomechanics and Thermal Pain. Springer.